Molecular Dynamics Simulations of a Polyalanine Octapeptide under Ewald Boundary Conditions: Influence of Artificial Periodicity on Peptide Conformation

Wolfgang Weber,[†] Philippe H. Hünenberger,[*,‡] and J. Andrew McCammon[†,⊥]

Department of Chemistry and Biochemistry and Department of Pharmacology, University of California at San Diego, 9500 Gilman Drive, La Jolla, California 92093-0365 and Laboratorium für Physikalische Chemie, ETH Zentrum, Universitätstrasse 6, CH-8092 Zürich, Switzerland

Received: October 25, 1999; In Final Form: January 25, 2000

Ewald and related mesh methods are nowadays routinely used in explicit-solvent simulations of solvated biomolecules, although they impose an artificial periodicity in systems which are inherently nonperiodic. In the present study, we investigate the consequences of this approximation for the conformational equilibrium of a polyalanine octapeptide (with charged termini) in water. We report three explicit-solvent molecular dynamics simulations of this peptide in cubic unit cells of edges $L = 2$, 3, and 4 nm, using the particle−particle−particle−mesh (P^3M) method for handling electrostatic interactions. The initial configuration of the peptide is α-helical. In the largest unit cell ($L = 4$ nm), the helix unfolds quickly toward configurations with shorter end-to-end distances. By contrast, in the two smaller unit cells ($L = 2$ and 3 nm), the α-helix remains stable during 2 ns. Backbone fluctuations are somewhat larger in the medium ($L = 3$ nm) compared to the smallest unit cell. These differences are rationalized using a continuum electrostatics analysis of configurations from the simulations. These calculations show that the α-helical conformation is stabilized by artificial periodicity relative to any other configuration sampled during the trajectories. This artificial stabilization is larger for smaller unit cells, and is responsible for the absence of unfolding in the two smaller unit cells and the reduced backbone fluctuations in the smallest unit cell. These results suggest that artificial periodicity imposed by the use of infinite periodic (Ewald) boundary conditions in explicit-solvent simulations of biomolecules may significantly perturb the potentials of mean force for conformational equilibria, and even in some cases invert the relative stabilities of the folded and unfolded states.

Introduction

The treatment of long-range electrostatic interactions in molecular simulations of liquids and solutions has been an area of active research for a long time.[1−6] The main reasons are that (i) this treatment generally represents the computationally most expensive part of a simulation and (ii) simulated observables are often extremely sensitive to approximations made in this treatment. During the past few years, the Ewald[7] and related mesh methods (P^3M[8] and PME[10]) to treat long-range electrostatic interactions in molecular simulations have been implemented in many of the widely used simulation packages (e.g., CHARMm, AMBER, NWChem). These methods are nowadays routinely used in explicit-solvent simulations of biomolecules[11−19] and may soon completely supersede the use of cutoff-based methods, which rely on the truncation of long-range electrostatic interactions. While the artifacts caused by cutoff truncation have been extensively studied[11−13,20−34] and shown to be severe in many cases, possible artifacts linked with the use of the Ewald and related mesh methods are just beginning to be understood.[6,35−42] Since the reliability of computer simulations may be significantly impaired by errors committed in the treatment of electrostatic interactions, it is of importance to assess also these methods with respect to the nature and magnitude of artifacts they may induce in various simulated observables.

Ewald and related mesh methods permit, in principle, the exact evaluation of electrostatic interaction energies and forces in systems with infinite periodic (Ewald) boundary conditions. However, whereas infinite translational symmetry is probably a good approximation for the simulation of crystals, it may prove a bad approximation for the simulation of liquids and solutions.[6,41,42] In particular, it can be expected that imposing artificial periodicity on liquids and solutions will represent a negligible perturbation when the unit cell is very large, but will drastically affect the properties of the system when small unit cells are used. The minimal size of the unit cell necessary to ensure a negligible periodicity-induced perturbation will depend on the nature of the system and on the observables of interest.

A number of studies suggested that artifacts linked with Ewald boundary conditions for the simulation of solutions are negligible. Among these, studies of the dependence of the potential energy on the orientation of small biomolecules within the unit cell indicated that Ewald rotational artifacts are small when a solvent of high permittivity is considered.[43,44] However, this conclusion may be restricted to solutes with a small solvent-excluded volume compared to the size of the unit cell.[42,45] A comparison of three 1.5 ns explicit-solvent simulations of a DNA dodecamer using the PME method and different numbers of water molecules[46] did not evidence a significant unit-cell size dependence of the monitored properties (root-mean-square deviation from the crystallographic structure and DNA curvature). This result may indicate the absence of artifacts linked with Ewald boundary conditions in this specific system, but this absence of artifacts may also simply be caused by a poor convergence or weak sensitivity of the selected observables.

* Corresponding author. E-mail: phil@igc.phys.chem.ethz.ch.
† Department of Chemistry and Biochemistry, University of California at San Diego.
‡ ETH Zentrum.
⊥ Department of Pharmacology, University of California at San Diego.

10.1021/jp9937757 CCC: $19.00
Published on Web 03/22/2000

Recently, we proposed a new method based on continuum electrostatics for assessing the nature and magnitude of periodicity-induced artifacts in explicit-solvent simulations under Ewald boundary conditions.[6,41,42] The principle of these calculations is the following. Ideally, one would like to perform a direct comparison between explicit-solvent simulations under nonperiodic and Ewald boundary conditions. This is impossible since an explicit-solvent system under nonperiodic boundary condition would be prohibitively large. However, a comparison between nonperiodic and Ewald boundary conditions becomes possible when an implicit representation of the solvent is used instead, e.g., by employing continuum electrostatics. Assuming that observations made using continuum electrostatics are (at least qualitatively) relevant for explicit-solvent simulations, this approach allows to investigate specifically the perturbation induced by artificial periodicity in simulations under Ewald boundary conditions.

In contrast to the previously mentioned studies,[43,44,46] the continuum electrostatics analysis of potentials of mean force for model conformational transitions of biomolecules indicated that artificial periodicity may significantly affect the result of biomolecular simulations.[6,42] The continuum electrostatics analysis of configurations from a nanosecond molecular dynamics (MD) simulation (using the P^{3}M method) of the protein Sac7d at 550 K[47] suggested that the anomalous stability of the protein during this simulation is (at least in part) a consequence of artificial periodicity.[42]

In the present work, we investigate whether the qualitative conclusions reached using the continuum electrostatics study of a model conformational transition can be confirmed by explicit-solvent MD simulations. Here, we focus on the case of a polyalanine octapeptide with charged termini, for which strong periodicity-induced artifacts were observed.[42] We report three explicit-solvent MD simulations of this peptide using the P^{3}M method for handling electrostatic interactions and employing three different unit cell sizes (cubes of edges $L = 2$, 3, and 4 nm). The effect of artificial periodicity on the conformational behavior of the peptide is analyzed in detail. It is then shown how the outcome of the simulations can be rationalized with the help of the continuum electrostatics analysis.

Theory

Using a continuum representation of the solvent, the free energy of a solute−solvent system may be partitioned into a sum of a nonpolar contribution, corresponding to the work required for creating the solute cavity in the solvent in the absence of solute charges, and an electrostatic contribution, corresponding to the work required for reversibly charging the solute atoms. Since the nonpolar contribution is dominated by short-range effects, we assume that the periodicity-induced perturbation of this contribution is negligible. Therefore, we focus on the perturbation imposed by artificial periodicity on the electrostatic contribution alone. This perturbation can be quantified as

$$\Delta\Delta G_{el} = [\Delta G_{el}]_P - [\Delta G_{el}]_{NP} \quad (1)$$

where $[\Delta G_{el}]_{NP}$ and $[\Delta G_{el}]_P$ are the electrostatic free energies of the solute−solvent system under nonperiodic and Ewald boundary conditions, respectively. As described elsewhere,[6,41,42] these quantities can be partitioned into two and three terms, respectively, as

$$[\Delta G_{el}]_{NP} = [E_{Cb}]_{NP} + [\Delta G_{solv}]_{NP} \quad (2)$$

and

$$[\Delta G_{el}]_P = [E_{Cb}]_P + [\Delta G_{self}]_P + [\Delta G_{solv}]_P \quad (3)$$

In practice, the solute is described as a low-dielectric cavity of relative permittivity ϵ_i immersed in a solvent of higher permittivity ϵ_s. The Coulomb terms E_{Cb} represent interactions between the partial charges on the solute atoms in a homogeneous medium of permittivity ϵ_i. The solvation terms ΔG_{solv} correspond to the work required for changing the external permittivity from ϵ_i to ϵ_s. Finally, the self-energy term ΔG_{self} (Ewald boundary conditions) corresponds to the sum of the self-energies of the charges plus homogeneous neutralizing background density (C + B charges[41]). A more detailed discussion of these different terms, together with numerical methods for their evaluation, is given elsewhere.[41]

Computational Details

Here, we investigate the unfolding equilibrium of a polyalanine octapeptide with charged N- and C-termini.

In a first step, we use the continuum electrostatics method to analyze the periodicity-induced perturbation of the electrostatic free energy (eq 1) along a model unfolding pathway. Peptide conformations along this pathway are generated using the dimensionless parameter λ, which defines the backbone φ and ψ angles of all residues through

$$\varphi(\lambda) = -57°(1 - \lambda) - 180° \lambda \quad \text{and}$$
$$\psi(\lambda) = -47°(1 - \lambda) - 180° \lambda \quad (4)$$

Other internal coordinates (bond lengths, bond angles, and improper dihedral angles) are fixed to standard values from the GROMOS96 force field.[48] The values $\lambda = 0$ and $\lambda = 1$ correspond to the canonical α-helix conformation and to the extended (all-trans) conformation, respectively. For all conformations, the three principal axes of the peptide are aligned with an edge of the unit cell. The periodicity-induced perturbation is calculated for cubic unit cells of edges $L = 2$, 3, and 4 nm. The parameters for these calculations are the same as for the analysis of the configurations from the MD simulations (see below).

In a second step, we report the results of explicit-solvent MD simulations of the peptide. These simulations were performed using the GROMOS96 force field[49] and a modified version of the GROMOS96 simulation program[48,50] incorporating the P^{3}M method[8] for handling electrostatic interactions. The initial configuration was taken to be the canonical α-helix (eq 4 with $\lambda = 0$). The solute was immersed in three different cubic unit cells containing 234, 866, and 2099 SPC water molecules[51] so that the edges of the corresponding unit cells were $L = 2$, 3, and 4 nm, respectively, with a solvent density of 1.0 g·cm^{-3}. In the starting configuration, the minimal distances between any solute atom and the nearest cell wall were 0.4, 1.4, and 2.4 nm, respectively. The three simulations were performed under Ewald boundary conditions using the P^{3}M method,[8] with a 1.0 nm cutoff distance for the real space contribution, a grid spacing of 0.05 nm, and a Gaussian charge-shaping function of width 0.3 nm. A 1.0 nm cutoff was used for the Lennard-Jones interactions. The nonbonded pair list was updated every 10 steps. The simulations were carried out in the NVT ensemble using a Berendsen thermostat[52] with separate solute and solvent coupling, a reference temperature of 300 K, and a relaxation time of 0.1 ps. Bond lengths were constrained using SHAKE[53] with a relative tolerance of 10^{-4}. A 2 fs time step was used to integrate the equations of motion, and coordinates were saved

every 0.1 ps for analysis. For equilibration, the system was heated to 300 K in steps of 100 K, each of 5 ps duration. Positional restraints of decreasing magnitude were applied simultaneously with the heating process. After equilibration, data were collected for 2 ns ($L = 2$ and 3 nm) or 1 ns ($L = 4$ nm).

For the analysis of the trajectories, we monitored the C_α root-mean-square atomic positional deviations (d_{rms}) with respect to the structure of the canonical α-helix, the C_α root-mean-square atomic positional fluctuations (f_{rms}), the hydrogen-bonding pattern, and the end-to-end distance (measured between the N-terminal ammonium nitrogen and the C-terminal carboxylate carbon). For the analysis of the hydrogen-bonding pattern, a hydrogen bond was assumed to be formed if the distance between the hydrogen and acceptor atoms was smaller than 0.25 nm and the angle between donor, hydrogen, and acceptor was larger than 135°. Hydrogen bonds corresponding to the α-helical configuration were numbered 1 through 4 according to the following definitions (residue numbers are indicated in parentheses): 1 = NH(5)→CO(1), 2 = NH(6)→CO(2), 3 = NH(7)→CO(3), and 4 = NH(8)→CO(4).

Finally, configurations sampled at 10 ps intervals during the three simulations were analyzed using the continuum electrostatics method to extract the periodicity-induced perturbation of the electrostatic free energy $\Delta\Delta G_{el}$ (eq 1). To this purpose, the electrostatic free energies under nonperiodic (eq 2) and Ewald (eq 3) boundary conditions were calculated as described previously[41,42] using a modified version of the UHBD program[54] with a grid spacing of 0.05 nm. The calculations under Ewald boundary conditions were performed using cubic unit cells of edges $L = 2$, 3, and 4 nm, as appropriate. For the calculations under nonperiodic boundary conditions, the edge lengths were augmented by a distance of 0.2 nm with respect to the value used in the simulation, in order to increase the distances between the solute atoms and the boundary of the grid.[42] Solute cavities were defined as the contact and reentrant surface obtained by rolling a probe of 0.14 nm radius over the peptide. For consistency, the atomic radii and charges were taken from the GROMOS96 force field.[48,49] The solute and solvent permittivities were set to $\epsilon_i = 1$ and $\epsilon_s = 78$, respectively.

Results and Discussion

First, we briefly discuss the results obtained from the analysis of the model unfolding pathway defined by eq 4. The periodicity-induced perturbation of the electrostatic free energy $\Delta\Delta G_{el}$ (eq 1) along this pathway is displayed in Figure 1 as a function of the end-to-end distance. The quantity $\Delta\Delta G_{el}$ is always negative and its absolute value increases with increasing end-to-end distance. Thus, artificial periodicity tends to destabilize the α-helical conformation relative to more extended structures. As shown by the different slopes of the curves corresponding to increasing edge lengths of the cubic unit cell ($L = 2$ nm to $L = 4$ nm), this effect becomes less important when the unit cell size is increased. This is not surprising since finite-size effects should vanish completely in the limit of an inifitely large unit cell.

As illustrated in Figure 2 for $L = 4$ nm, the trends in $\Delta\Delta G_{el}$ result from the balance between two opposing effects.[42] On the one hand, the Coulomb contributions $[E_{Cb}]_{NP}$ and $[E_{Cb}]_P + [\Delta G_{self}]_P$ (Figure 2a) decrease with increasing end-to-end distance, because the unfavorable interaction between the backbone dipole and the charged termini decreases in magnitude when the peptide unfolds. The shift in the Coulomb contribution caused by artificial periodicity is negative and its absolute value increases in magnitude with increasing end-to-end distance. This shift is due to the favorable interaction between the charged termini of the oligopeptide and those of its periodic copies in adjacent unit cells. On the other hand, the solvation contributions $[\Delta G_{solv}]_{NP}$ and $[\Delta G_{solv}]_P$ (Figure 2b) are negative and their absolute values decrease with increasing end-to-end distance. The shift in the solvation contribution caused by artificial periodicity is positive and increases in magnitude with increasing

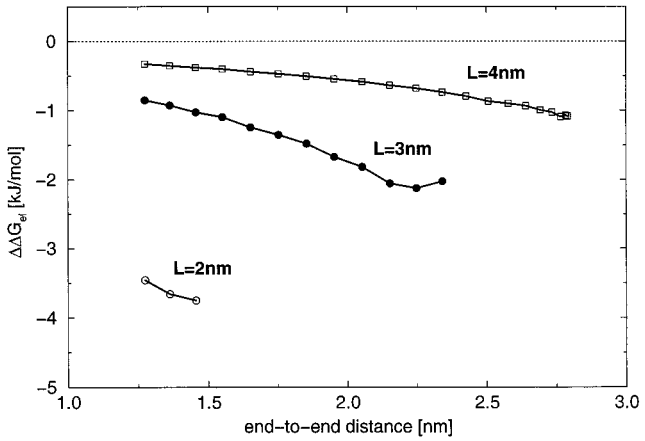

Figure 1. Periodicity-induced perturbation of the electrostatic free energy $\Delta\Delta G_{el}$ (eq 1), for a polyalanine octapeptide (charged termini), along the model unfolding pathway defined by eq 4. The end-to-end distance is measured between the N-terminal ammonium nitrogen and the C-terminal carboxylate carbon. Curves are displayed for cubic unit cells of edges $L = 2$, 3, and 4 nm. The calculations were performed as described in ref 42, using the GROMOS96 charges and radii.[48,49] These curves differ from those reported in ref 42 and result from more accurate calculations.

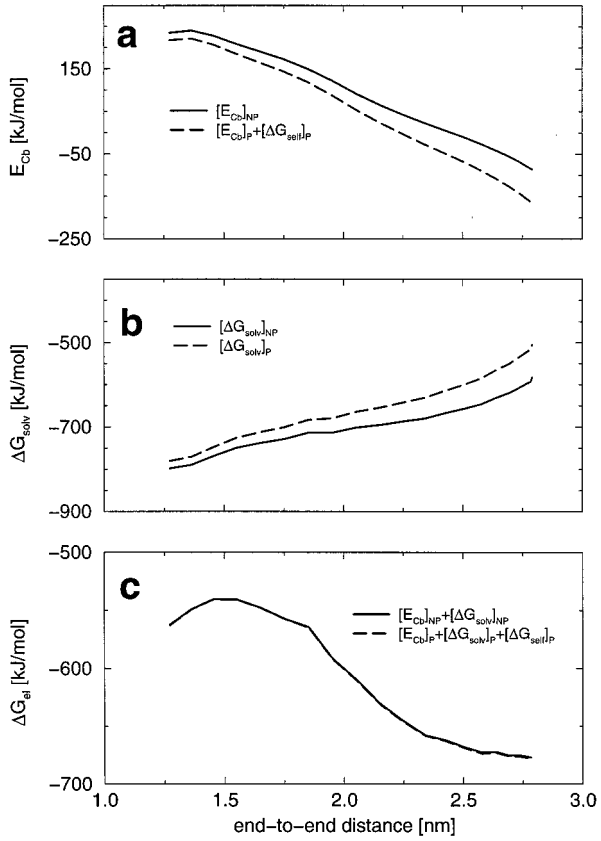

Figure 2. Coulomb (a) and solvation (b) contributions to the electrostatic free energy (c) calculated under nonperiodic (NP) or Ewald (P) boundary conditions (see eqs 2 and 3) for a polyalanine octapeptide (charged termini), along the model unfolding pathway defined by eq 4. Curves are displayed for a cubic unit cell of edge $L = 4$ nm.

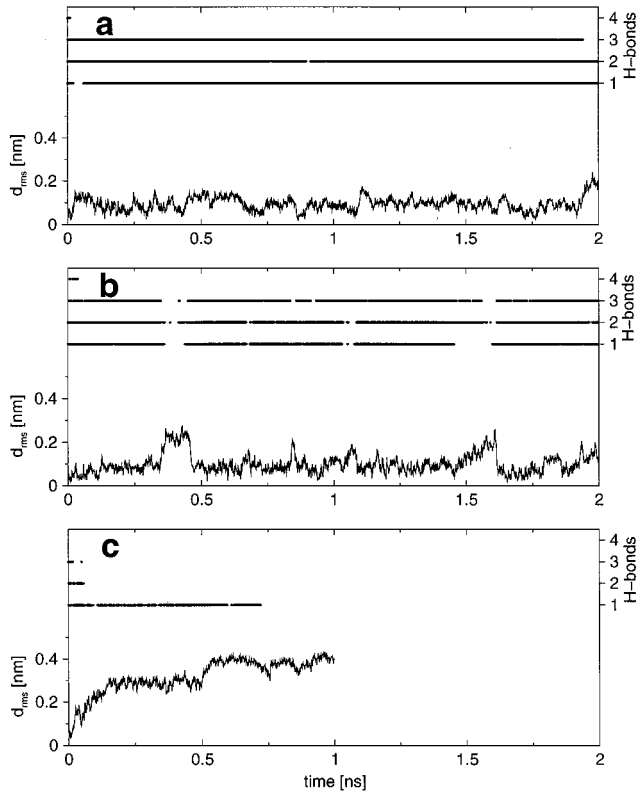

Figure 3. C_α root-mean-square atomic positional deviation (d_{rms}) from the canonical α-helix (lower panels) and hydrogen-bonding pattern (upper panels), from the MD simulations with cubic unit cells of edges $L = 2$ (a), 3 (b), and 4 nm (c). The hydrogen bond numbering scheme is (residue numbers are given in parentheses): 1 = NH(5)→CO(1), 2 = NH(6)→CO(2), 3 = NH(7)→CO(3), and 4 = NH(8)→CO(4).

end-to-end distance. This shift may be viewed as a consequence of the perturbation of the solvent by the periodic copies of the oligopeptide, which renders the solvent less available for the solvation of the oligopeptide in the central unit cell. This effect increases in magnitude with the size of the overall dipole moment of the peptide, i.e., with the end-to-end distance. The sum of the Coulomb and solvation contributions, i.e., the total electrostatic contribution to the potential of mean force, is shown in Figure 2c for nonperiodic and Ewald boundary conditions. This total electrostatic contribution strongly favors extended conformations relative to the α-helix. Note, however, that the overall potential of mean force depends on additional covalent, nonpolar, and entropic contributions, so that no direct conclusion can be drawn on which conformations will dominate at equilibrium. The large periodicity-induced shifts in the Coulomb and solvation contributions (Figure 2a,b) cancel each other to a large extent, resulting in a much smaller periodicity-induced shift of the overall electrostatic free energy (Figure 2c). The periodicity-induced shift in the Coulomb contribution (favoring extended structures) still slightly dominates over the corresponding shift in the solvation contribution (favoring the α-helix), resulting in the trends observed in Figure 1.

To check whether these qualitative observations reached using continuum electrostatics applied to a model unfolding pathway can be verified in explicit-solvent MD simulations, we now discuss the results of three explicit-solvent MD simulations of the octapeptide in cubic unit cells of edges $L = 2$, 3, and 4 nm, and using the P^3M method for handling electrostatic interactions. The time evolutions of the C_α root-mean-square atomic positional deviation (d_{rms}, lower panels) and of the hydrogen-bonding pattern (upper panels) are displayed in Figure 3 for the three simulations. For the $L = 2$ nm simulation, d_{rms} remains relatively low (about 0.1 nm) and fluctuates little over the 2 ns simulation time. The same observation applies to the $L = 3$ nm simulation, except for two excursions to higher values (about 0.25 nm) in the intervals 0.35−0.45 and 1.50−1.60 ns. By contrast, the value of d_{rms} during the $L = 4$ nm simulation increases rapidly to about 0.4 nm within the first 0.6 ns of the simulation. A qualitative difference can also be observed between the hydrogen-bonding patterns corresponding to the three simulations. While the C-terminal hydrogen bond 4 is disrupted very early in all cases, the three other α-helical hydrogen bonds are only preserved during the $L = 2$ and 3 nm simulations. For $L = 2$ nm, hydrogen bonds 1, 2, and 3 are present for 90%, 88%, and 82% of the configurations, respectively. Hydrogen bonds characteristic of a 3_{10}-helix (not shown in the figure), such as NH(5)→CO(2), NH(6)→CO(3), and NH(7)→CO(4), also occur during this simulation, but are formed in less than 5% of the configurations. For $L = 3$ nm, hydrogen bonds 1, 2, and 3 are present for 75%, 76%, and 67% of the configurations, respectively. Transient disruptions of these three hydrogen bonds coincide with the two peaks observed in d_{rms} around 0.40 and 1.55 ns. Here, 3_{10}-helix hydrogen bonds are slightly more frequent (5−10% of the configurations). In addition, the hydrogen bonds NH(6)→CO(1) and NH(7)→CO(2) replace the α-helical ones around 0.40 and 1.55 ns. For $L = 4$ nm, the initial α-helical hydrogen bonds are disrupted after about 0.06 ns (bonds 2 and 3) and 0.73 ns (bond 1). No other type of hydrogen bond occurs for more than 5% of the configurations, except for the hydrogen bond NH(7)→CO(1) present from 0.75 ns until the end of the simulation.

The end-to-end distance of the peptide is displayed as a function of time in Figure 4 (upper panels). For the simulations in the two smallest unit cells, the end-to-end distance remains close to the initial value of 1.27 nm (canonical α-helix), as could be expected from Figure 3. By contrast, for $L = 4$ nm, an initial increase of the end-to-end distance during the first 0.1 ns is followed by a rapid decrease to lower values in the range 0.3−1.1 nm, compatible with the existence of the NH(7)→CO(1) hydrogen bond. The periodicity-induced perturbation of the electrostatic free energy $\Delta\Delta G_{el}$ (eq 1) is also displayed in Figure 4 (lower panels). Three observations can be made here: (i) $\Delta\Delta G_{el}$ is always negative; (ii) it decreases in magnitude with increasing unit cell size; (iii) it is strongly anti-correlated with the end-to-end distance. The latter point is particularly evident in the $L = 4$ nm simulation where the octapeptide undergoes a significant conformational change. These three observations are in perfect agreement with the results obtained from the study of the model unfolding pathway (Figure 1).

Ten superimposed configurations sampled at 100 ps intervals during each of the three simulations are shown in Figure 5. The corresponding C_α root-mean-square atomic positional fluctuations (f_{rms}) are displayed in Figure 6. For $L = 2$ nm, as could be anticipated from Figures 3a and 4a, the peptide remains very stable in the α-helical conformation. The corresponding backbone fluctuations are small (0.04−0.06 nm for the C_α of residues 1−7). For $L = 3$ nm, the peptide also remains stable in the α-helical conformation. However, the backbone fluctuations are somewhat higher (0.07−0.09 nm for the C_α of residues 1−7) and transient disruption of α-helical hydrogen bonds are observed (Figure 3b). By contrast, for $L = 4$ nm, the peptide is completely unfolded after about 0.7 ns (Figure 3c), and the backbone fluctuations are significantly higher than in the two previous cases. Since the configurations from the last 0.3 ns of this simulation lack any hydrogen bond except for NH(7)→CO-

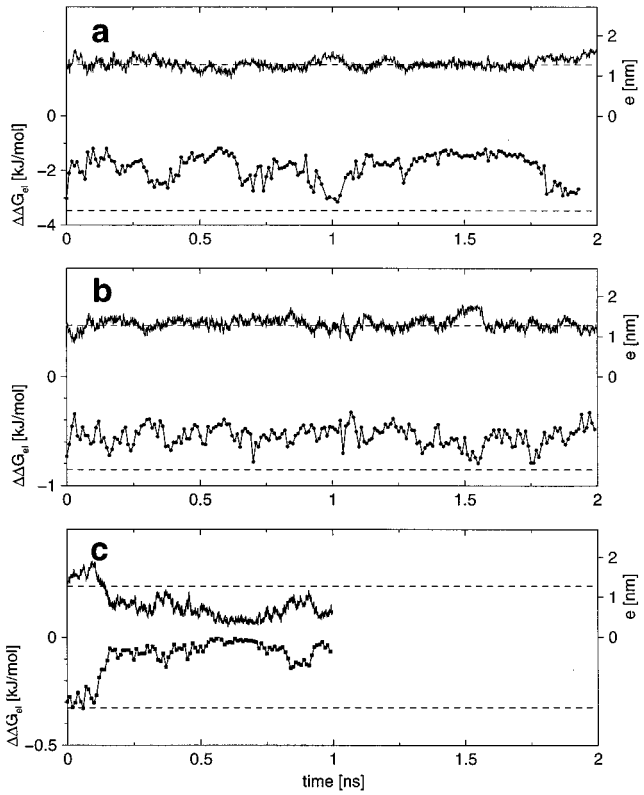

Figure 4. Periodicity-induced perturbation of the electrostatic free energy $\Delta\Delta G_{el}$ (lower panels), according to eq 1, and end-to-end distance e (upper panels), from MD simulations with cubic unit cells of edges $L = 2$ (a), 3 (b), and 4 nm (c). Dashed lines represent the $\Delta\Delta G_{el}$ and e values characteristic of the α-helix: $e = 1.27$ nm and $\Delta\Delta G_{el} = -3.46$ ($L = 2$ nm), -0.85 ($L = 3$ nm), and -0.33 kJ/mol ($L = 4$ nm). For the calculation of $\Delta\Delta G_{el}$ using continuum electrostatics, the configurations were translated but not rotated, and the same unit cell sizes were used as during the corresponding simulation.

(1) and have a short end-to-end distance (Figure 4c) so that the two charged termini are almost in direct contact (Figure 5c), we will refer to these as "circle" conformations. Note that in contrast to the simplistic unfolding pathway used in the initial continuum electrostatics study (Figure 1), where unfolding was interpreted as an increase in the end-to-end distance, unfolding in the $L = 4$ nm simulation leads to circle conformations with shorter end-to-end distances compared with the α-helix. Except for this important difference, the results of the explicit-solvent MD simulations and of the continuum calculations on the model unfolding pathway are in very good qualitative agreement, as discussed below.

The cause for the different conformational behavior of the polypeptide chain in the three simulations can be easily understood by considering Figure 7. This figure shows, for the conformations sampled at 10 ps intervals during the three simulations, the correlation between the periodicity-induced perturbation of the electrostatic free energy $\Delta\Delta G_{el}$ (calculated using the continuum method) and the end-to-end distance. The points representative for the canonical α-helix and for a typical circle configuration (sampled at 0.8 ns during the $L = 4$ nm simulation) are also represented. Note the similarity between Figures 1 and 7 in terms of the slopes of the correlations for the three different unit cell sizes. As discussed above (see Figure 4), the absolute value of $\Delta\Delta G_{el}$ decreases with both a decreasing end-to-end distance and an increasing unit cell size. The periodicity-induced destabilization of the circle configuration relative to the canonical α-helix evaluates to 2.8 ($L = 2$ nm), 0.7 ($L = 3$ nm), and 0.3 kJ/mol ($L = 4$ nm). Configurations which are penalized by a perturbation of the order of (or greater than) $k_BT = 2.5$ kJ/mol at 300 K are essentially inaccessible during the MD simulation. For $L = 2$ nm, the free energy corresponding to configurations with shorter end-to-end distances (compared to the α-helix) is strongly affected by artificial periodicity. Since the circle configurations are penalized by about 2.8 kJ/mol (greater than k_BT), they are essentially inaccessible during the MD simulation. For $L = 3$ nm, $\Delta\Delta G_{el}$ as well as the slope of the correlation line are smaller in magnitude, and the circle configurations are penalized by only about 0.7 kJ/mol. Consequently, configurations with shorter end-to-end distances become more accessible, although not to the extent of permitting unfolding within the 2 ns simulation. On the other hand, fluctuations in the peptide backbone become more important (Figure 6). For $L = 4$ nm, the periodicity-induced perturbation becomes small enough to permit unfolding toward the (thermodynamically more stable) circle configuration. The behavior of the peptide in this latter simulation is probably the most relevant for comparison with experiment, since the perturbation due to artificial periodicity is the smallest in this case. Indeed, it is known experimentally that oligopeptides of such short lengths do not adopt a stable α-helical conformation.[55] Note finally that the quality of the correlation between $\Delta\Delta G_{el}$ and the end-to-end distance improves in the sequence $L = 2$ nm (correlation coefficient $r = -0.52$), $L = 3$ nm ($r = -0.73$), and $L = 4$ nm ($r = -0.94$). This can be understood as follows. In the largest box, periodicity-induced artifacts are caused primarily by the interaction between the peptide in the central unit cell and its periodic copies in the two adjacent cells along the peptide axis, and thus are well correlated with the end-to-end distance. On the other hand, in the smallest box, the interaction between the peptide and its periodic copies in the other four adjacent cells becomes more important (because these copies are now only about 2 nm away), and the correlation with the end-to-end distance becomes worse.

The above explanation for the different conformational behaviors of the peptide during the three simulations rests on the hypothesis that the circle configuration is thermodynamically favored over the α-helical one. However, it is difficult to distinguish whether periodicity-induced artifacts cause these different behaviors for thermodynamic or kinetic reasons. If the thermodynamic explanation holds, the free energy difference between circle and helical conformations must be small enough that the periodicity-induced perturbation in the smallest unit cells is suffient to inverse the relative stabilities of the two conformations. If the kinetic explanation holds, the periodicity-induced perturbation in the smallest unit cells only slows down sampling in the direction of the favored circle configuration, so that this configuration is not observed during a nanosecond simulation. Considering the magnitude of the periodicity-induced perturbation (Figure 7), the thermodynamic explanation seems more likely in the $L = 2$ nm case, whereas the kinetic explanation is probably correct for $L = 3$ nm. This point could be addressed in more detail by performing longer simulations. Note finally that the peptide is never observed to unfold toward extended configurations, even though these would be significantly stabilized by artificial periodicity in the smallest boxes. This probably simply reflects the intrinsic thermodynamic instability of these configurations in the case of an octapeptide with charged termini.

Another possible explanation for the absence of unfolding in the two smaller unit cells (and especially for $L = 2$ nm) could be the lack of space, i.e., the presence of short-range packing contacts between the peptide in the central unit cell and its

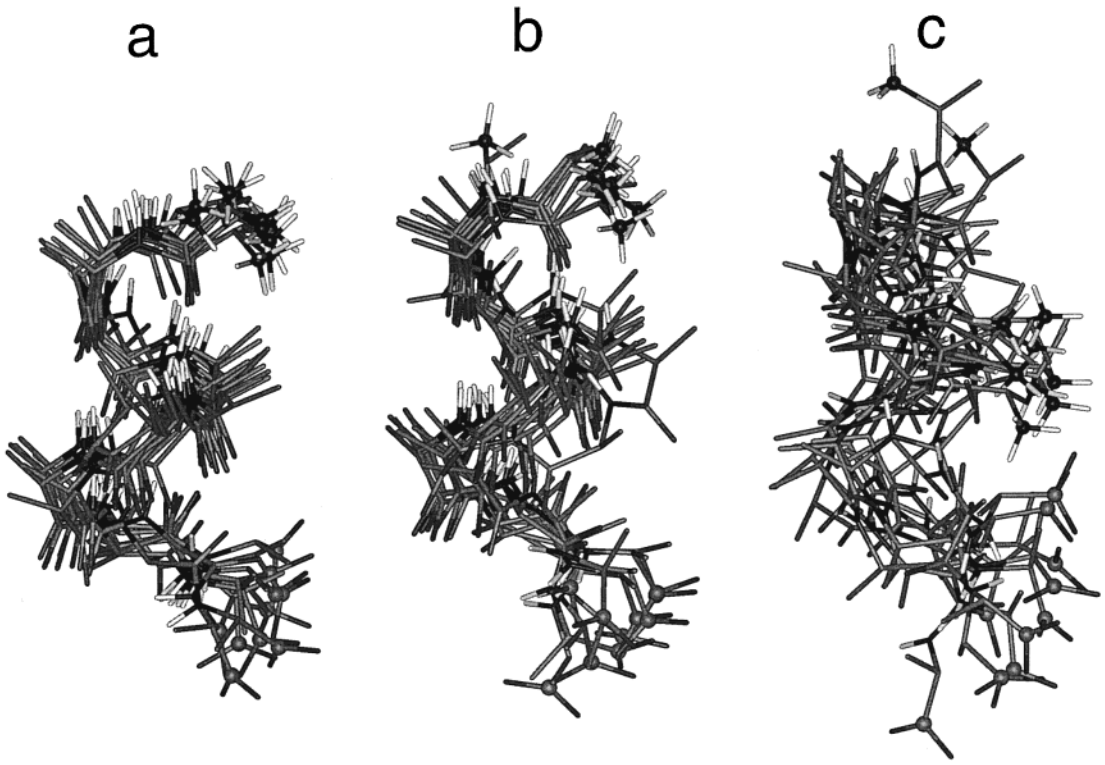

Figure 5. Ten configurations (superimposed on the C_α atoms) taken at 100 ps intervals from the three MD simulations with cubic unit cells of edges $L = 2$ (a), 3 (b), and 4 nm (c).

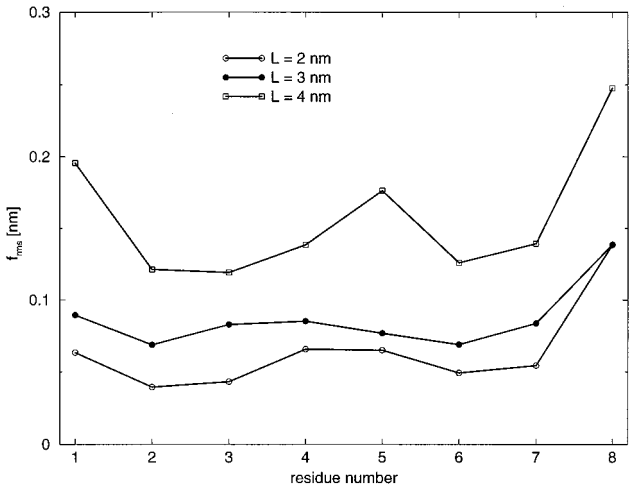

Figure 6. C_α root-mean-square atomic positional fluctuations (f_{rms}) corresponding to the eight residues of the octapeptide, calculated from the first 1 ns of the three MD simulations with cubic unit cells of edges $L = 2$, 3, and 4 nm.

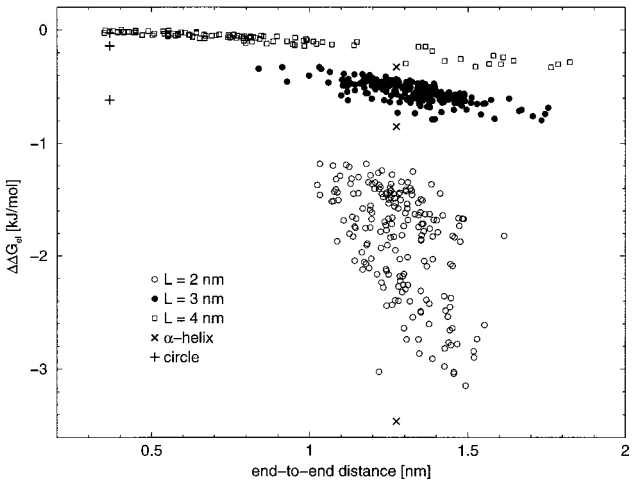

Figure 7. Periodicity-induced perturbation of the electrostatic free energy $\Delta\Delta G_{el}$ (eq 1) calculated from configurations sampled at 10 ps interval during the three MD simulations with cubic unit cells of edges $L = 2$, 3, and 4 nm. Values corresponding to the canonical α-helix (×) and to a model circle configuration (+) are also represented (from bottom to top $L = 2$, 3, and 4 nm). The model circle configuration is the configuration sampled at 0.8 ns during the MD simulation with $L = 4$ nm. See also Figure 4.

periodic copies. However, this explanation can easily be ruled out. The maximal values of the end-to-end distance in the three simulations are (see Figure 4) 1.69 ($L = 2$ nm), 1.78 ($L = 3$ nm), and 1.85 nm ($L = 4$ nm), which is always at least 0.3 nm smaller than the edge length of the unit cell, and at least 1.7 nm smaller than the diagonal of the cell ($\sqrt{3}L$). In fact, for the $L = 2$ nm simulation, the distance between the N-terminus of the peptide in the central unit cell and the C-terminus of any of its periodic copies is always larger than 0.5 nm, and larger than 0.75 nm in 90% of the configurations. Furthermore, the fact that the unfolding observed in the $L = 4$ nm simulation proceeds with a maximal end-to-end distance of 1.85 nm indicates that this pathway would be feasible in the $L = 2$ nm unit cell without involving any packing contacts. Thus, the reason for the absence of unfolding in the two smaller unit cells is not the presence of packing contacts within the periodic system, but rather the effect of the periodicity-induced perturbation of the electrostatic interactions.

Conclusion

In the present study we investigated artifacts linked with the use of Ewald boundary conditions in explicit-solvent simulations of a polyalanine octapeptide with charged termini. This was done by comparing the results of three explicit-solvent MD simulations of the peptide using the P^3M method and cubic unit cells of different sizes ($L = 2$, 3, and 4 nm). These

simulations, initiated using the α-helical conformation, were analyzed in terms of the conformational behavior of the peptide chain.

Experimentally, peptides of such a small size are known not to adopt stable helical conformations in water at room temperature.[55] Our results show that indeed, under the most realistic simulation conditions (i.e., in the largest unit cell of edge L = 4 nm), the α-helix unfolds quickly. The peptide was found to adopt circle configurations in which the two charged termini are in close proximity and no hydrogen bonds are present except for NH(7)→CO(1). By contrast, during the simulations in the two smaller unit cells (L = 2 and 3 nm), which are more significantly affected by finite-size effects, the α-helix remained stable over the simulation times of 2 ns. The two latter simulations differed in terms of the flexibility of the peptide backbone, which was found to be more pronounced in the L = 3 nm simulation.

The different conformational behavior of the peptide observed in these three MD simulations was rationalized using a continuum electrostatic analysis of configurations sampled during the simulations. Such calculations[6,41,42] permit estimation of the periodicity-induced perturbation of the electrostatic free energy $\Delta\Delta G_{el}$ (eq 1) by comparing the electrostatic free energies of the solute−solvent system under nonperiodic and Ewald boundary conditions. The analysis of $\Delta\Delta G_{el}$ for the three different simulations showed that the canonical α-helix is stabilized by artificial periodicity relative to all other configurations sampled during the trajectories. In particular, the α-helix is stabilized relative to the circle configurations encountered in the L = 4 nm simulation after unfolding. This periodicity-induced destabilization was estimated to be about 2.8 (L = 2 nm), 0.7 (L = 3 nm), and 0.3 kJ/mol (L = 4 nm). This perturbation appears sufficient to prevent (either thermodynamically or kinetically) the unfolding in the L = 2 and 3 nm simulations. Furthermore, it significantly reduces the backbone fluctuations in the L = 2 nm simulation. Only for L = 4 nm is the perturbation sufficiently small so that unfolding readily occurs.

These results suggest that artificial periodicity imposed by the use of Ewald boundary conditions in explicit-solvent simulations may significantly perturb the potentials of mean force for conformational equilibria of solvated biomolecules. In the case of the polyalanine octapeptide and in the two smaller unit cells (L = 2 and 3 nm), the perturbation may even be strong enough to inverse the relative stabilities of the circle and α-helical conformations. Considering the L = 4 nm system as a reference, it appears that periodicity-induced artifacts can be made essentially negligible by sufficiently solvating the peptide during the setup of the simulation. For this specific system, we would recommend the inclusion of at least three solvation layers (about 0.85 nm) between the peptide termini and the nearest unit-cell walls. In fact, such a requirement is not unrealistically drastic for the simulation of typical biomolecules.

Considering the results of the present study, we suggest that explicit-solvent simulations of biomolecular systems under Ewald boundary conditions should be systematically examined for periodicity-induced artifacts. The continuum electrostatics analysis proposed previously[6,41,42] appears to be an appropriate (qualitative) tool for this purpose. From this and previous studies,[41,42] periodicity artifacts are likely to be important (k_BT or larger) for systems involving (i) a solvent of low dielectric permittivity, (ii) few solvation shells around the solute, and (iii) a solute bearing a net charge or a large dipole. In particular, the periodicity artifacts observed in the present study would probably be negligible in the case of an octapeptide with neutral termini.[42]

However, in the long run, we also hope that the realization that periodicity-induced artifacts are sometimes far from negligible will trigger the development of more accurate lattice-sum methods for handling long-range interactions in simulations.

Acknowledgment. P.H.H. acknowledges support from the Swiss National Science Foundation and the Human Frontier Science Program. Additional support was provided by NIH and NSF. This work was also partially supported by the NSF Supercomputer Centers NRAC program.

References and Notes

(1) Harvey, S. C. *Proteins: Struct. Funct. Genet.* **1989**, *5*, 78.
(2) Davis, M.E.; McCammon, J.A. *Chem. Rev.* **1990**, *90*, 509.
(3) Smith, P.E. In *Computer simulation of biomolecular systems, theoretical and experimental applications*; van Gunsteren, W. F., Weiner, P. K., Wilkinson, A. J., Eds.; ESCOM: Leiden, The Netherlands, 1993; Vol. II, pp 182−212.
(4) Levy, R. M.; Gallicchio, E. *Annu. Rev. Phys. Chem.* **1998**, *49*, 531.
(5) Sagui, C.; Darden, T. A. *Annu. Rev. Biophys. Biomol. Struct.* **1999**, *28*, 155.
(6) Hünenberger, P. H. In *Simulation and theory of electrostatic interactions in solution: Computational chemistry, biophysics, and aqueous solutions*; Pratt, L. R., Hummer, G., Eds.; American Institute of Physics: New York, 1999; pp 17−83.
(7) Ewald, P. P. *Ann. Phys.* **1921**, *64*, 253.
(8) Hockney, R. W.; Eastwood, J. W. *Computer simulation using particles*; Institute of Physics Publishing: Bristol, 1988.
(9) Darden, T.; York, D.; Pedersen, L. *J. Chem. Phys.* **1993**, *98*, 10089.
(10) Essmann, U.; Perera, L.; Berkowitz, M. L.; Darden, T.; Lee, H.; Pedersen, L. G. *J. Chem. Phys.* **1995**, *103*, 8577.
(11) Smith, P. E.; Pettitt, B. M. *J. Chem. Phys.* **1991**, *95*, 8430.
(12) Schreiber, H.; Steinhauser, O. *Biochemistry* **1992**, *31*, 5856.
(13) Schreiber, H.; Steinhauser, O. *Chem. Phys.* **1992**, *168*, 75.
(14) York, D. M.; Darden, T. A.; Pedersen, L. G. *J. Chem. Phys.* **1993**, *99*, 8345.
(15) Fox, T.; Kollman, P. A. *Proteins: Struct. Funct. Genet.* **1996**, *25*, 315.
(16) Mohan, V.; Smith, P. E.; Pettitt, B. M. *J. Phys. Chem.* **1993**, *97*, 12984.
(17) Cheatham III, T. E.; Kollman, P. A. *J. Mol. Biol.* **1996**, *259*, 434.
(18) Young, M. A.; Ravishanker, G.; Beveridge, D. L. *Biophys. J.* **1997**, *73*, 2313.
(19) Auffinger, P.; Westhof, E. *Curr. Opin. Struct. Biol.* **1998**, *8*, 227.
(20) Neumann, M. *Mol. Phys.* **1983**, *50*, 841.
(21) Neumann, M.; Steinhauser, O.; Pawley, G. S. *Mol. Phys.* **1984**, *52*, 97.
(22) Wood, R. H. *J. Chem. Phys.* **1995**, *103*, 6177.
(23) Brooks III, C. L.; Pettitt, B. M.; Karplus, M. *J. Chem. Phys.* **1985**, *83*, 5897.
(24) Baker, N. A.; Hünenberger, P. H.; McCammon, J. A. *J. Chem. Phys.* **1999**, *110*, 10679.
(25) Brooks III, C. L. *J. Chem. Phys.* **1987**, *86*, 5156.
(26) Madura, J. D.; Pettitt, B. M. *Chem. Phys. Lett.* **1988**, *150*, 105.
(27) Straatsma, T. P.; Berendsen, H. J. C. *J. Chem. Phys.* **1989**, *89*, 5876.
(28) Pettitt, B. M.; Rossky, P. J. *J. Chem. Phys.* **1986**, *84*, 5836.
(29) Dang, L. X.; Pettitt, B. M. *J. Phys. Chem.* **1990**, *94*, 4303.
(30) Guàrdia, E.; Rey, R.; Padró, J. A. *J. Chem. Phys.* **1991**, *95*, 2823.
(31) Dang, L. X.; Pettitt, B. M.; Rossky, P. J. *J. Chem. Phys.* **1992**, *96*, 4046.
(32) Hummer, G.; Soumpasis, D. M.; Neumann, M. *Mol. Phys.* **1993**, *81*, 1155.
(33) Bader, J. S.; Chandler, D. *J. Phys. Chem.* **1992**, *96*, 6423.
(34) Schreiber, H.; Steinhauser, O. *J. Mol. Biol.* **1992**, *228*, 909.
(35) Figueirido, F.; Del Buono, G. S.; Levy, R. M. *J. Chem. Phys.* **1995**, *103*, 6133.
(36) Hummer, G.; Pratt, L. R.; Garcia, A. E. *J. Phys. Chem.* **1996**, *100*, 1206.
(37) Figueirido, F.; Del Buono, G. S.; Levy, R. M. *J. Phys. Chem. B* **1997**, *101*, 5622.
(38) Hummer, G.; Pratt, L. R.; Garcia, A. E. *J. Chem. Phys.* **1997**, *107*, 9275.

(39) Hummer, G.; Pratt, L. R.; Garcia, A. E. *J. Phys. Chem. A* **1998**, *102*, 7885.
(40) Sakane, S.; Ashbaugh, H. S.; Wood, R. H. *J. Phys. Chem. B* **1998**, *102*, 5673.
(41) Hünenberger, P. H.; McCammon, J. A. *J. Chem. Phys.* **1999**, *110*, 1856.
(42) Hünenberger, P. H.; McCammon, J. A. *Biophys. Chem.* **1999**, *78*, 69.
(43) Smith, P. E.; Pettitt, B. M. *J. Chem. Phys.* **1996**, *105*, 4289.
(44) Smith, P. E.; Blatt, H. D.; Pettitt, B. M. *J. Phys. Chem. B* **1997**, *101*, 3886.
(45) Luty, B. A.; van Gunsteren, W. F. *J. Phys. Chem.* **1996**, *100*, 2581.
(46) Norberto de Souza, O.; Ornstein, R. L. *Biophys. J.* **1997**, *72*, 2395.
(47) de Bakker, P. I. W.; Hünenberger, P. H.; McCammon, J. A. *J. Mol. Biol.* **1999**, *285*, 1811.
(48) van Gunsteren, W. F.; Billeter, S. R.; Eising, A. A.; Hünenberger, P. H.; Krüger, P.; Mark, A. E.; Scott, W. R. P.; Tironi, I. G. *Biomolecular simulation: The GROMOS96 manual and user guide*; Verlag der Fachvereine: Zürich, 1996.
(49) Daura, X.; Mark, A. E.; van Gunsteren, W. F. *J. Comput. Chem.* **1998**, *19*, 535.
(50) Scott, W. R. P.; Hünenberger, P. H.; Tironi, I. G.; Mark, A. E.; Billeter, S. R.; Fennen, J.; Torda, A. E.; Huber, T.; Krüger, T.; van Gunsteren, W. F. *J. Phys. Chem. A* **1999**, *103*, 3596.
(51) Berendsen, H. J. C.; Postma, J. P. M.; van Gunsteren, W. F.; Hermans, J. In *Intermolecular Forces*; Pullman, B., Ed., Reidel: Dordrecht, 1981; pp 331−342.
(52) Berendsen, H. J. C.; Postma, J. P. M.; van Gunsteren, W. F.; Haak, J. R. *J. Chem. Phys.* **1984**, *81*, 3684.
(53) Ryckaert, J.-P.; Ciccotti, G.; Berendsen, H. J. C. *J. Comput. Phys.* **1977**, *23*, 327.
(54) Madura, J. D.; Davis, M. E.; Gilson, M. K.; Wade, R. C.; Luty, B. A.; McCammon, J. A. In *Reviews in computational chemistry*; Lipkowitz, K. B., Boyd, D. B., Eds.; VCH Publishers, Inc.: New York, 1994; pp 229−267.
(55) Chakrabartty, A.; Baldwin, R. L. *Adv. Protein Chem.* **1995**, *46*, 141.